p-ISSN 2089 – 0133 e-ISSN 2477-6416 Indonesian Journal of Applied Physics (IJAP) Vol. 12 No. 1 page 124
URL : https://jurnal.uns.ac.id/ijap/article/view/49179 DOI : https://doi.org/10.13057/ijap.v12i1.49179

PERFORMANCE CHARACTERIZATION OF 450 NM VISIBLE LIGHT BASED PHOTOACOUSTIC IMAGING FOR PHANTOM IMAGING OF SYNTHETIC DYE CONTRAST AGENTS

Mahendra Kusuma Nugraha*, Moh. Ali Joko Wasono and Mitrayana
Department of Physics, Faculty of Mathematics and Natural Science, Gadjah Mada University, Yogyakarta, Indonesia
*mahendrakusuma@mail.ugm.ac.id

Received 09-03-2021, Revised 19-01-2022, Accepted 01-02-2022
Available Online 17-03-2022, Published Regularly April 2022

ABSTRACT

Performance characterization of 450 nm visible light photoacoustic imaging has been carried out through phantom imaging of methylene blue (MB), methyl orange (MO), and methyl red (MR) dye solutions. The phantom was made of a nylon tube with a diameter of 5.0 mm (outside) and 4.6 mm (inside) having a height of 2.0 mm along with a 6×6 cm black galvanized aluminum plate as the background medium. The nylon tube was filled with each type of solution with varying molecular concentrations of 10, 25, 50 and 100 ppm. Twelve (12) phantom objects were imaged in an area of 10×10 cm. The visible absorption peak known from UV-Visible spectroscopy for each type of solution is at 664 nm (methylene blue), 465 nm (methyl orange), and 522 nm (methyl red). It was also known that the amplitude of PA emissions would increase proportionally to the concentration of dye molecules. Overall, methyl orange solutions had the highest photoacoustic emission amplitude distribution. The analysis showed that the ratio of inner diameter (ID) and wall thickness (WT) between the MB and MO phantom images to the original object were 1:0.83 and 1:0.74 (ID) and 1:3 and 1:1.5 (WT), respectively. On the other hand, the ratio of the outer diameter (OD) of the MR phantom image to the original object is 1:1.28.

Keywords: photoacoustic imaging; visible light; diode laser; phantom; photoacoustic contrast agent; dye solution.

INTRODUCTION

Nowadays, photoacoustic imaging (PAI) is a well-known type of non-ionizing radiation-based imaging modality. Observations from Zhu et al. (2018) stated that photoacoustic imaging has been developed extensively during the last few decades, especially for its application in clinical and biomedical fields[1].

One of many causes behind the increasing development of photoacoustic imaging was presented by Attia et al. (2019) and Steinberg et al. (2019) which stated that photoacoustic imaging modality can provide some good quality images of biological tissues with decent optical contrast and spatial resolution[2,3]. PAI modalities are also considered to have a sufficient level of depth penetration for internal organs/sub-skin imaging purposes[4].

Three years earlier, Weber et al. (2016) put forward that PAI modalities (especially in infrared PAI systems ranging from 620-950 nm) can penetrate and image up to several

centimetres below the object.[5] The known spatial resolution values range from about μm to cm. Based on many findings above, it is undeniable that photoacoustic imaging can be developed significantly in a short period. Until now, PAI modalities have been used to image various biological objects, both animals and humans, starting from oral soft tissues[6], brain[3], and mice prostate[7]. PAI has also been known to image various kinds of human tumour cells (glioblastoma U-87MG and epidermoid carcinoma A431)[8].

In recent years, photoacoustic imaging has shifted from using conventional class-IV laser sources such as Nd: YAG[1,9]and OPO[10] to contemporary lasers such as semiconductor diodes (pulsed laser diodes; PLD) and even LED arrays. Semiconductor diode lasers are considered to be more reliable, practical, durable, cheap, and easy to operate than class-IV lasers[1,9,11]. Thus, the use of these semiconductor diodes and LEDs paved the way for the development of visible light-based photoacoustic imaging (visible PAI systems). However, the imaging depth of visible PAI systems ranging from 400-700 nm is generally lower than the infrared-based ones (700-1100 nm). This condition is caused by the use of visible light sources characterized by shorter wavelengths so that it tends to be more susceptible to scattering by biological objects or tissues.[4] It has also been shown that—in special cases—the excitation energy intensity coming from an LED-PAI system is two orders of magnitude smaller compared to the energy coming from class-IV laser sources. This results in object/ tissue images generated by the related PAI system having a relatively low signal-to-noise value[1].

To overcome those exceptions, it's necessary to have increased efficiency by optimizing the performance and imaging capabilities of the intended visible light PAI system. One of many methods to achieve more reliable images from visible light sources in PAI is by involving the use of external/exogenous photoacoustic contrast agents. Based on many experimental results, the utilization of exogenous contrast agents proved to be able to optimize: (i) contrast difference and image resolution quality; (ii) imaging depth (axial resolution); and (iii) detection sensitivity of photoacoustic signals[12–14]. Not only those, Weber et al. (2016) even depicted that the utilization of exogenous contrast agents can help visualize the occurrence of biological processes in the body with decent precision. Among various types of photoacoustic contrast agents including nanoparticles, fluorescent synthetic dyes are the most common type of contrast agents used in PAI modalities for medical and research purposes[5, 13]. For example, two kinds of synthetic dyes have proven their effectiveness through various studies: indocyanine green (ICG)[8, 15] and methylene blue[15,16].

This experiment is intended to find out the suitability and decency of dye contrast agents when implemented in a 450 nm diode laser visible light photoacoustic imaging system. Three types of dye contrast agents selected in this experiment include methylene blue (MB; $C_{16}H_{18}ClN_3S$), methyl orange (MO; $C_{14}H_{14}N_3NaO_3S$) and methyl red (MR; $C_{15}H_{15}N_3O2$). To facilitate characterization and imaging procedure, the dyes are fabricated into a simple-shaped imaging phantom based on nylon plastic material. The expected output from this research was a representation of experimental data that embodied the performance and capability of the 450 nm visible light-based PAI system to image the three types of dye contrast agents.

METHODS

PAI SYSTEM CALIBRATION

The visible PAI system utilized in this experiment consist of three main hardware components. The audio sonic transducer used for detecting incoming PA emission was a single omnidirectional Behringer® ECM8000 condenser microphone. Along with it, the Behringer® U-PHORIA UMC202 HD soundcard was chosen as DAQ hardware. By this device, the photoacoustic waves detected by the microphone were converted into electrical signals which could be further processed and interpreted to represent two-dimensional photoacoustic images. The third main component was a semiconductor diode that acted as the 1000 mW 450 nm visible laser source. Utilizing a TTL logic function available in the system, the laser intensity could be modulated into certain frequencies to pave the PA generation from the object.

This PAI system utilized a Raspberry Pi 4B microcomputer to accommodate all of the hardware components (microphone, laser, monitor, etc.) with various supporting software to form an integrated photoacoustic imaging software that could be accessed via the microcomputer interface. The mentioned Raspberry Pi 4B microcomputer used a Debian Linux-based (Ubuntu®) operating system. Therefore, the latter obtained PA images could be directly observed and analyzed as displayed on the monitor. Before any imaging experiment was conducted, the utilized visible PAI system needed to be calibrated before to ensure all of the substantial components worked properly. Two measurements made up the calibration procedure which was the frequency response measurement and the laser power stability measurement. The first one was done to discover the microphone sensitivity level in detecting sound waves in different frequencies. On other hand, the emission energy intensity coming from the laser source had to be stable to achieve a good quality assurance on the obtained PA images. The laser power stability was measured using Field Best - Optical Power Meter from Fast Laser Tech®. Figure 1 shows the general schematic of our PAI system.

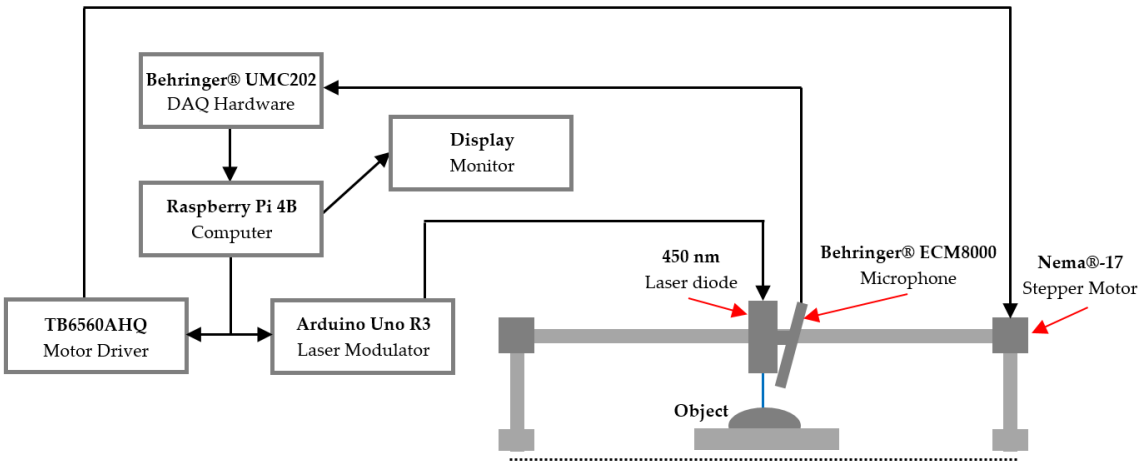

Figure 1. Schematic of the 450 nm visible light-based PAI system with the functional diagram of every main component.

To produce images, the system used a general two-dimensional scanning method in which the image pixels are continuously acquired from every specific point on the horizontal X and Y-axis of the object. The interval size or the step size between one point to another

was 0.2 mm. During the scan, the transducer runs from the top left side towards the bottom right side of the imaging area with 250 ms delay time between each pixel as illustrated in Figure 2 below.

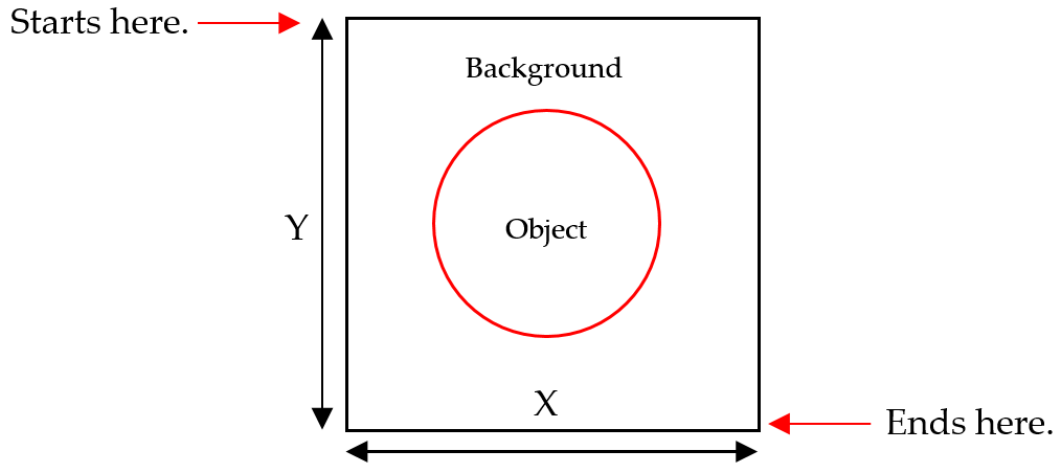

Figure 2. Depiction of the two-dimensional (2D) image scanning method used along with its axes in the mentioned visible PAI system.

SAMPLE FABRICATION AND PHANTOM CHARACTERIZATION

The first step began by diluting each of the dye solutions using the appropriate solvent, which was aqua distillate or distilled water (H_2O). The purpose was to obtain a variety of specific concentration values (M_i) for each type of dye solution. The mentioned specific concentration value (M_i) could be determined by utilizing the given mathematical equation:

$$M_i = \frac{M_0 \times V_0}{(V_i + V_0)} \qquad (1)$$

Referring to Eq. (1), $M_0$and V_0 were the initial volume (mL) and concentration (ppm) of the solution, respectively. The expression $(V_i + V_0)$ represented the latter volume of the solution, where V_i was the solvent volume (mL) used for the dye dilution process. The concentration of each type of dye solution determined in this experiment was 10 ppm, 25 ppm, 50 ppm and 100 ppm whereas the initial concentration was 5000 ppm (methylene blue) and 1000 ppm (methyl orange and methyl red). After that, each of them that had been diluted onto a specific level of concentration was slowly injected into a 5.0 mm nylon tube having a height of 2.0 mm using a 1 mL syringe. The relatively small size of the tube required the filling process to be done carefully to prevent spillage. Next, the twelve (12) nylon tubes containing each of those solutions were then placed side by side according to their concentration level onto a homogenous background medium made of a 6×6 cm galvalume thin plate coated with black metal paint. The determined spacing between the tubes was about 10 mm. Finally, the tubes along with the background medium were then placed inside a 95 mm transparent borosilicate petri dish which acted as a container.

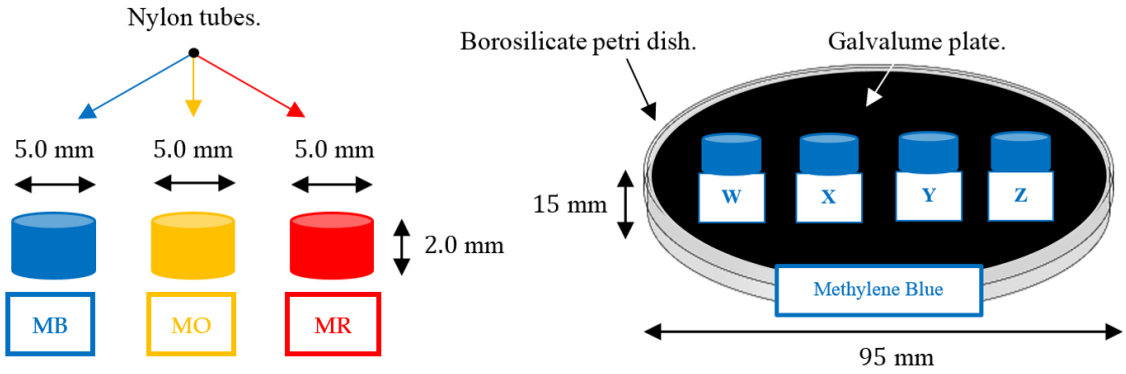

Figure 3. Design of the dye solution-based simple photoacoustic imaging phantom with black-painted galvanized aluminum plate as background medium.

ABSORPTION PEAKS CHARACTERIZATION

This procedure aimed to find out the absorbance strength characteristics on the visible light spectrum for each previously fabricated synthetic dye solution. The utilized instrument was the Shimadzu® UV-1800 which had detection wavelengths ranging from 200 to 800 nanometers. The detection limit of this spectrophotometer was about ~1 nm.

PHOTOACOUSTIC AMPLITUDE CHARACTERIZATION

Before acquiring the phantom images, it was prominent to determine two of the input parameters, which were the optimum intensity modulation frequency (v_m) and duty cycle percentage ($D_{\%}$) of the laser used to image the object. This procedure needed to be done to achieve feasible PA images because the quality of the images was fairly dependent on those two input parameters above.

In the first step, each of the phantom sets containing every specific concentration of dye solution was placed onto the imaging plane. Then, a certain surface point on each phantom was exposed by a modulated laser beam with different modulation frequencies (v) ranging from 15 to 20 kHz for a specific percentage of duty cycle (30%, 40%, 50%, and 60%) and was carried out for a certain amount of time. Afterwards, the resulting PA emissions coming from the object were detected by a condenser microphone positioned 70° perpendicular to the imaging plane/stage.

Furthermore, the acquired PA signals were processed by the system's software to represent the measured acoustic intensity level (T_I) generated by the PA effect on each corresponding phantom. Then, the average acoustic intensity level (T_I) obtained from repeated measurements were linearly mapped together for each of the corresponding modulation frequency values.

PA IMAGES ACQUISITION

Right after the optimum input parameters had been achieved, it was time to conduct the phantom imaging procedure using the referred 450 nm visible light PAI system. This stage was done to understand the performance and feasibility of the system to image both of each three different types of synthetic dye solutions and the 5.0 mm nylon tubes which acted as containers for the dye compounds. The selected two-dimensional imaging area (A) in this phantom imaging experiment was about 10×10 mm with pixel scanning time (t) around 250 ms.

PA IMAGES ANALYSES

The last procedure was to carry out further analysis on the acquired PA images. First, it was to investigate the pattern that lies in the one dimensional cross-sectional PA amplitude profile of each image that had been obtained before. Moreover, this procedure was done to ascertain the system's capability to accurately image the object by conducting a comparative analysis on the geometry of the real object versus the geometry of the obtained PA image.

RESULT AND DISCUSSION

HARDWARE PERFORMANCE CALIBRATION

Based on the analysis of the related interpretation, it can be stated that, in general, the microphone detection sensitivity level represented by the acoustic intensity level (SPL_d) tends to differ from one specific frequency value to another. The above statement is proven by the acquisition of the average sound intensity level (SPL_m) which is almost entirely different for each variation of the given reference acoustic frequency.

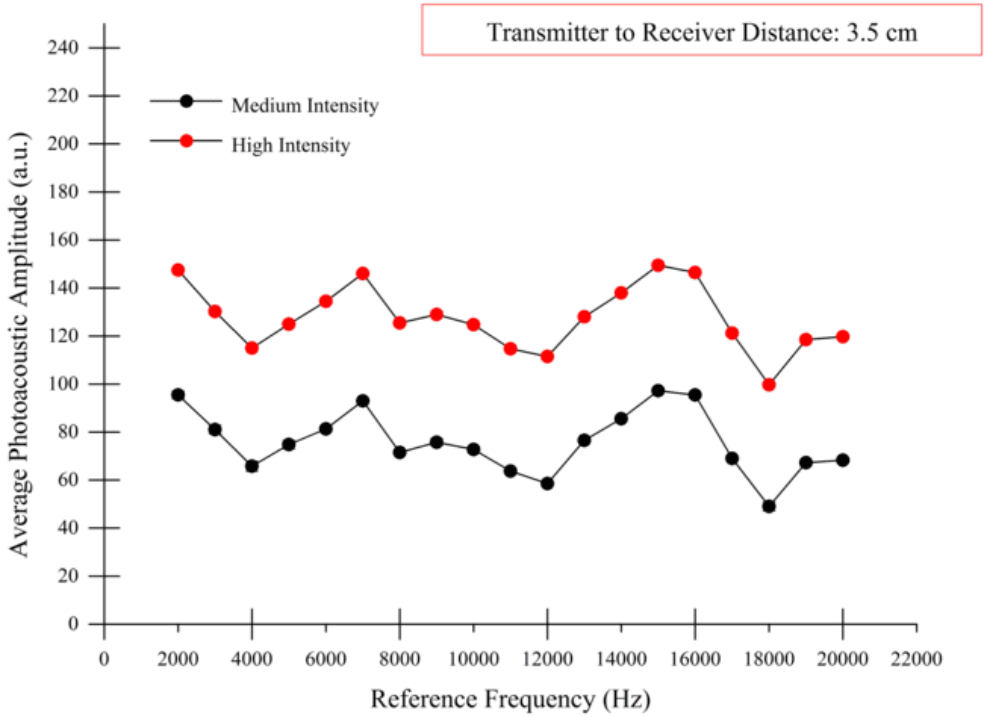

Figure 4. Frequency response of Behringer® ECM8000 condenser microphone.

From Figure 4, it can also be observed that the microphone has the highest detection sensitivity at 7000 and 15000 Hz. On the other hand, the lowest detection sensitivity is at 4000, 12000, and 18000 Hz. Further observation shows that the microphone detection sensitivity range with the minimum difference is at 8000 to 12000 Hz. In this range, the difference in the average sound intensity level measured for each reference frequency input (v_r) is not very significant between one another.

It has to be known that the Behringer® ECM8000 microphone is a type of condenser microphone that operates within the audio sonic frequency range ($20 - 20000$ Hz). Therefore, it is appropriate that this type of microphone tends to amplify acoustic signals

(soundwave) at certain frequencies. Such condition results in the difference acoustic detection sensitivity level between one frequency and another.

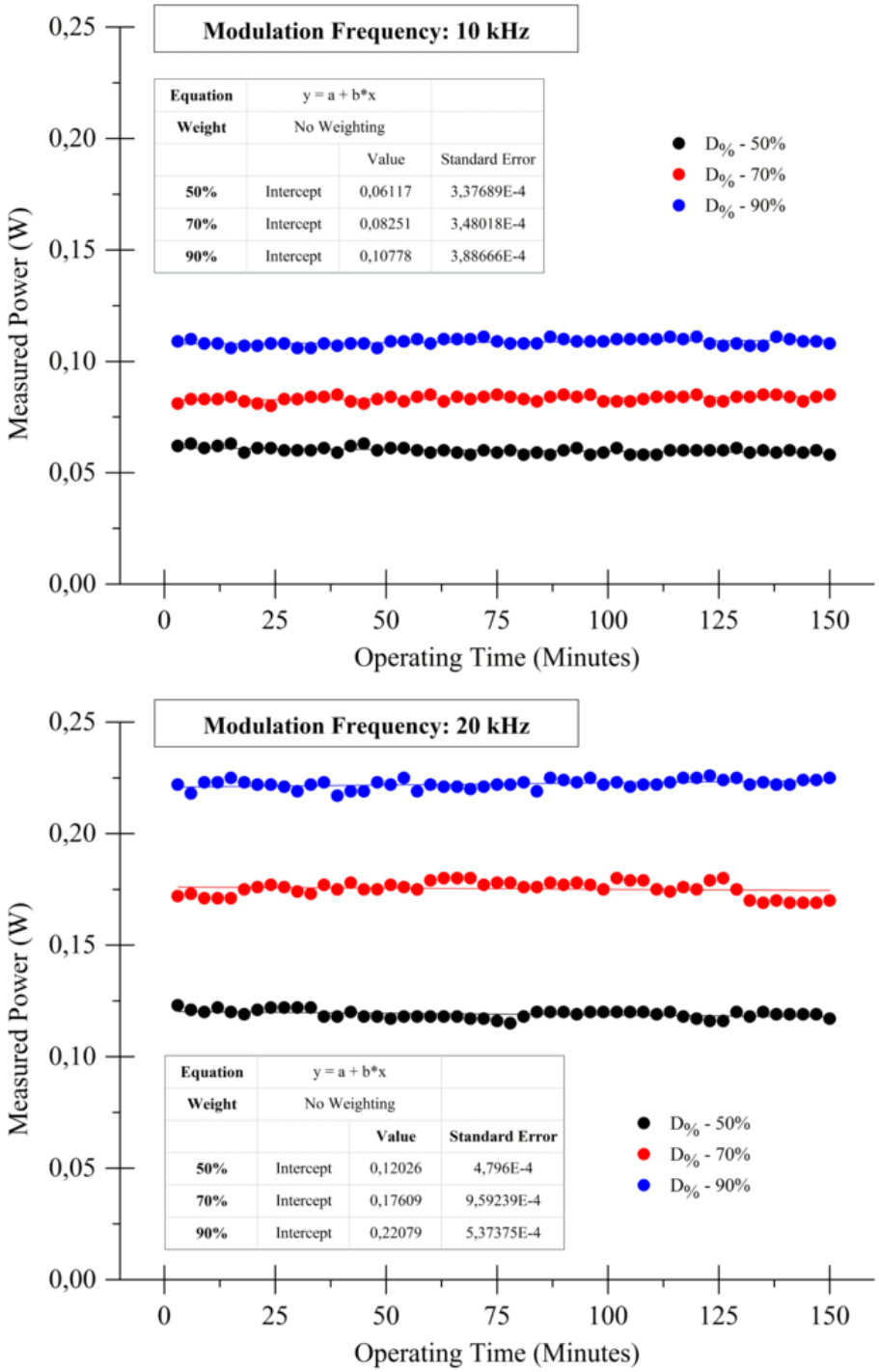

Figure 5. Emission power characteristics versus laser operating time at 10 kHz (top) and 20 kHz (bottom) modulation frequency.

The emission stability measurement as referred to above was done by measuring the laser radiation power (P_m) every three (3) minutes interval for a total of 150 minutes operating time. This calibration procedure also considers the effect of different values on the input parameters (modulation frequency and duty cycle percentage). The acquired

measurement data was then presented in the form of a linear graph. As shown in Figure 5, it can be observed that the emission power is quite stable over the operating period (150 minutes). The y-intercept (b) value obtained from the linear fitting is very close to the average measured radiation power (P_{mean}) obtained for every specified duty cycle percentage ($D_{\%}$). For example, at 10 kHz modulation frequency, the approximate y-intercept (b) value for $D_{\%}$: 90% is ~0.1078 (shown in Figure 5). On the other hand, the average measured radiation power for the same duty cycle percentages is around ~0.1087 mW.

Summary of the overall analysis shows no significant fluctuation between one measured power value to another during the emission stability calibration process. In addition, the obtained standard deviation (σ) is also quite negligible for each input parameter involved. For example, the standard deviation values (σ) at 10 kHz intensity modulation frequency are 0.0013 ($D_{\%}$: 50%; and 70%) and 0.0014 ($D_{\%}$: 90%). Thus, it can be stated the radiation power emitted from the semiconductor diode used as the laser source in this experiment is sufficiently stable.

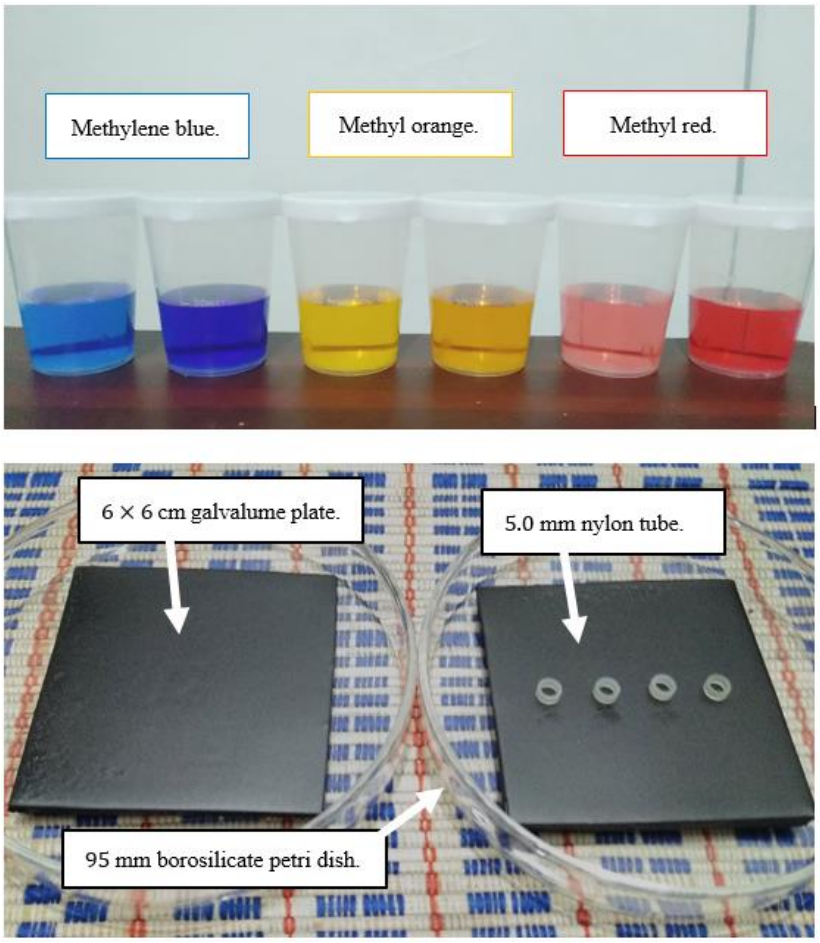

Figure 6. Few of several solutions of each dye compound after being diluted to the desired concentration (top). Image of the mentioned dye solution-based photoacoustic phantoms with 6 × 6 cm black galvanized aluminum plate as background medium before (left) and after (right) placement of 5.0 mm nylon tubes (bottom).

SAMPLE PREPARATION AND CHARACTERIZATION

Figure 6 above shows several examples of the three types of dye solution that had gone through the dilution process to the desired concentration and the mentioned dye solution-based photoacoustic phantoms with 6×6 cm black galvanized aluminum plate as background medium before and after placement of 5.0 mm nylon tubes.

UV-Visible spectroscopy result on each dye solution with a concentration level of 10 ppm and 25 ppm as shown in Figure 7 indicates that the highest peak absorption wavelength (λ_{peak}) of 10 ppm and 25 ppm MB solutions is at 664 and 651 nm respectively. Also, several other absorption peaks are lower at 613 nm (10 ppm) and 611 nm (25 ppm). According to the National Center for Biotechnology Information (2020), the absorption wavelength (λ_{abs}) of methylene blue is in the range 608-668 nm.

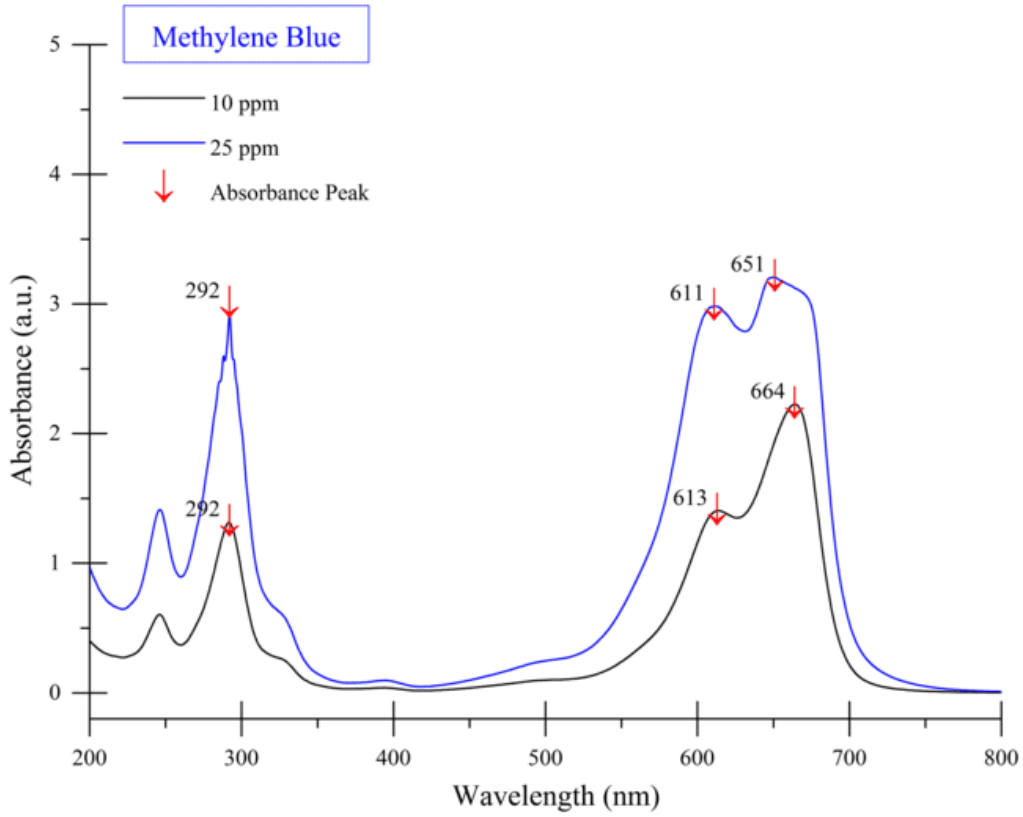

Figure 7. Visible light absorbance characteristics of methylene blue solutions.

On the other hand, the presented Figure 8 and Figure 9 below respectively show the absorption peak wavelength of 25 ppm methyl orange and methyl red solution which are at 465 and 522 nm. According to Falaras et al. (2003), the peak absorption wavelength of methyl orange is around 466.5 nm.[17] As for methyl red, reference data from National Center for Biotechnology Information (2020) shows a peak absorption wavelength at 521 nm. Therefore—based on a comparative analysis of each dye compound—it can be stated that the obtained absorption wavelength (λ_{abs}) measurement is relevant to the existing references.

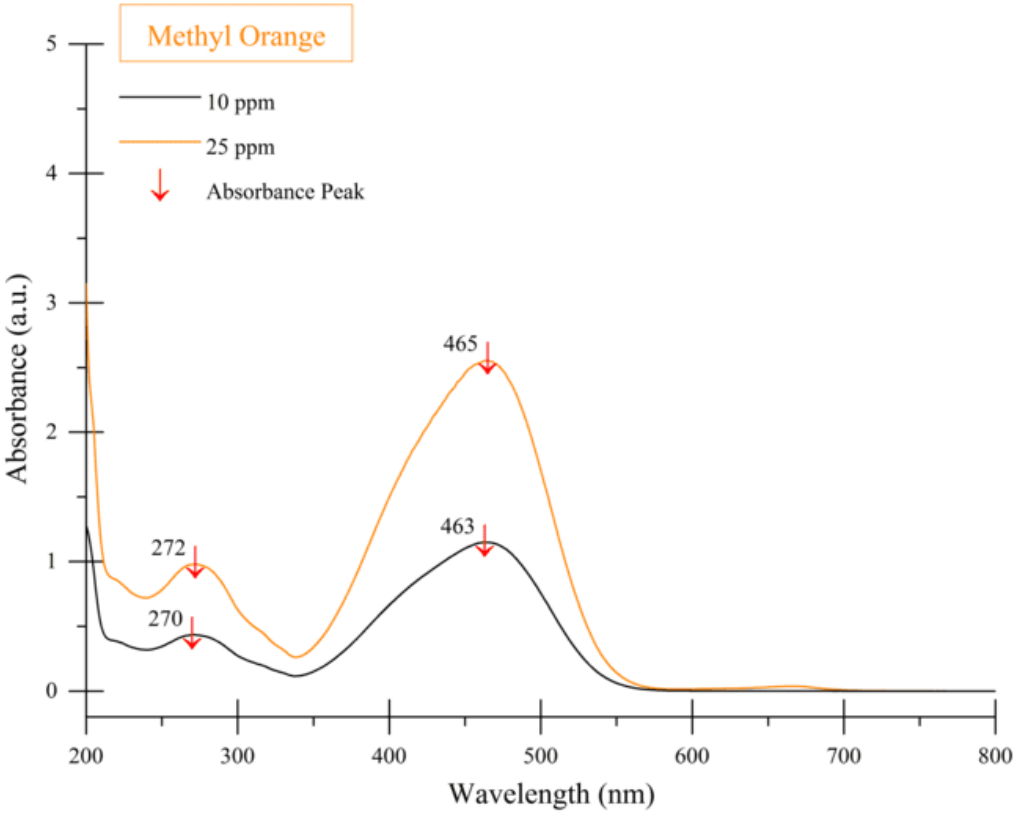

Figure 8. Visible light absorbance characteristics of methyl orange solutions.

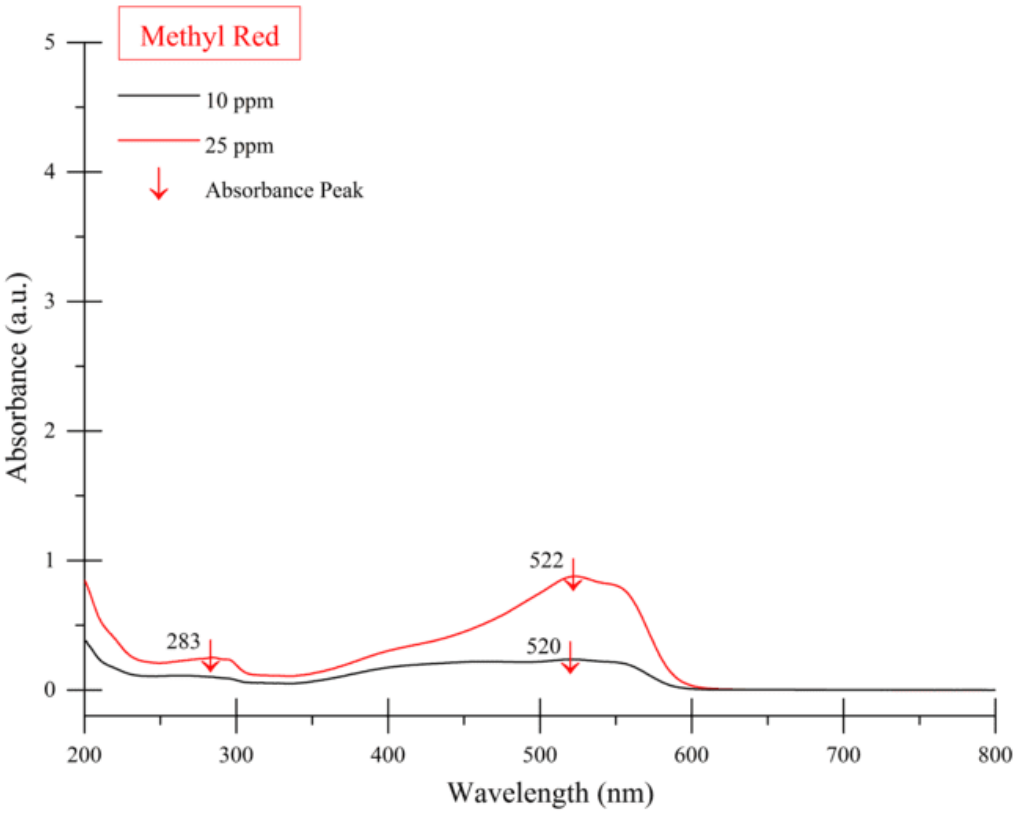

Figure 9. Visible light absorbance characteristics of methyl red solutions.

Acoustic intensity level (T_I) measurement on 100 ppm methylene blue (MB) solution (Figure 10) shows that the average value detected by the microphone varies in line with the increasing modulation frequency. The presented data also shows that the maximum measured acoustic intensity is achieved at 20000 Hz, which is compatible with the theoretical basis. Also, it seems that the greater duty cycle percentage contributes more to the average intensity emitted from the object regardless of the difference in modulation frequency input.

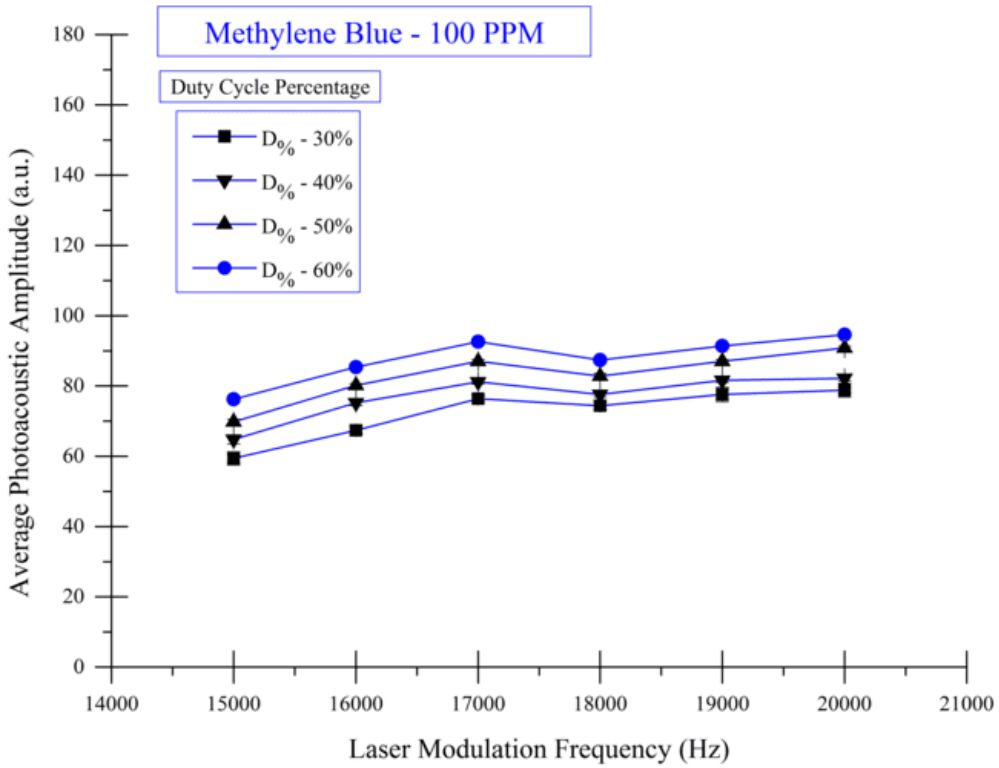

Figure 10. Measured photoacoustic emission amplitude in 100 ppm methylene blue solution.

The average acoustic intensity level (T_I) obtained from 100 ppm methyl red solution (MR) also describes a similar pattern (shown in Figure 11). However, the achieved maximum measured acoustic intensity is slightly higher than the one obtained from methylene blue. The different maximum value as mentioned above is believed to emerge due to the absorbance properties of methyl red (≅520 nm) which is stronger on the laser emission wavelength at 450 nm compared to methylene blue (≅650 nm).

On the other side, the acquired T_I feature from 100 ppm methyl orange (MO) solution shows a more progressive pattern than the two previous samples (Figure 12). The measured value seems to increase swiftly proportional to the modulation frequency magnitude. Under average conditions, the pattern is continuous from 15 (min. value) to 20 kHz (max. value). However, there is a slight decrease at 18 kHz before rising again. The swift increase in measured average acoustic intensity level as presented in Figure 9. is also believed to happen due to the absorbance properties of methyl orange (≅465 nm) which is very strong on the laser emission wavelength. Because of that, the photoacoustic effect occurrence probability resulting from the absorption of modulated electromagnetic radiation is increased so that the average acoustic intensity detected by the microphone is

also intense. These findings have proven that the absorbance properties of each dye compound directly influence the magnitude of the measured average acoustic intensity.

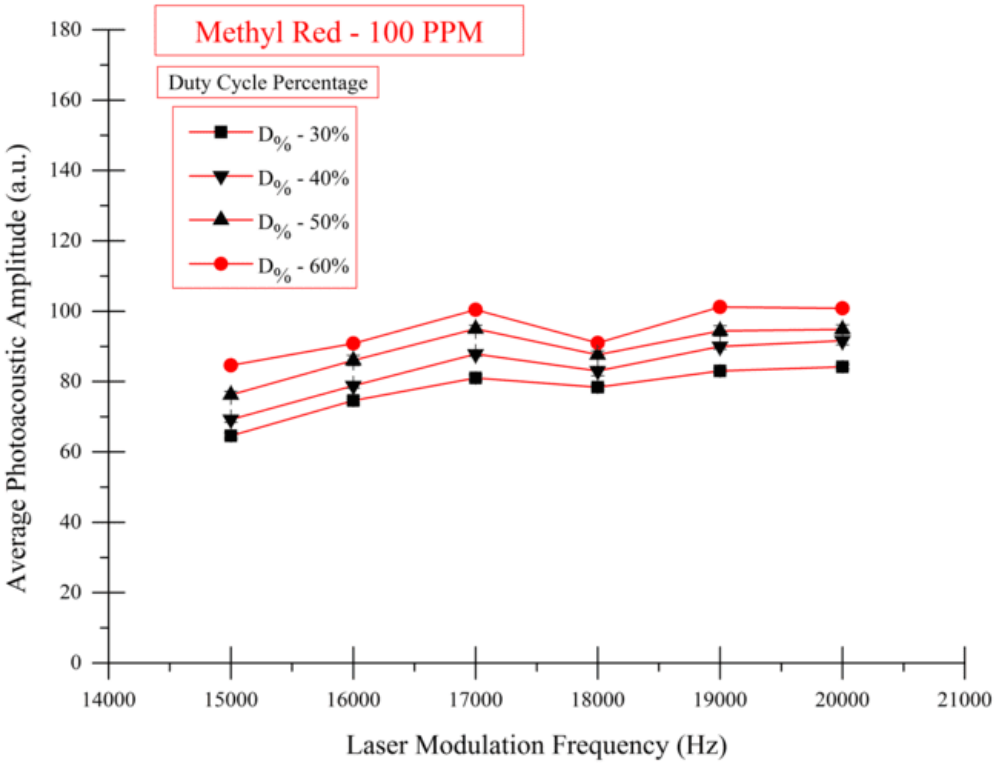

Figure 11. Measured photoacoustic emission amplitude in 100 ppm methyl red solution.

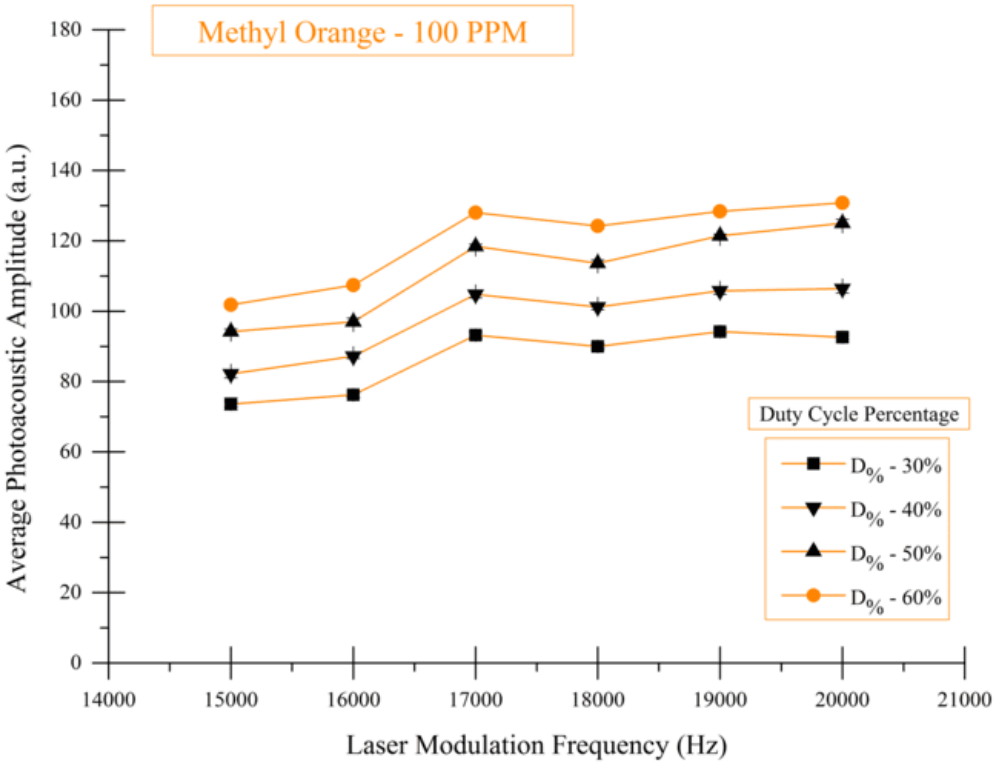

Figure 12. Measured photoacoustic emission amplitude in 100 ppm methyl orange solution.

IMAGES ACQUISITION AND ANALYSES

The number of phantoms imaged in this experiment was twelve (12) objects, where each type of dye solution has four different concentration levels which are 10, 25, 50 and 100 ppm. Figure 13 shows the photographic image of a 1.0 × 1.0 cm two-dimensional cross-sectional imaging area that covers the phantom object as well as the background medium. The pixel scanning time (t) was set to ≈ 250 ms. The microphone was positioned 3.0 cm from the object with a ≈ 70° angle perpendicular to it. Geometry measurement revealed that the phantom had an outer diameter of 5.00 ± 0.05 mm, an inner diameter of 4.60 ± 0.05 mm, a wall thickness of 0.40 ± 0.05 mm and a height of 2.00 ± 0.05 mm.

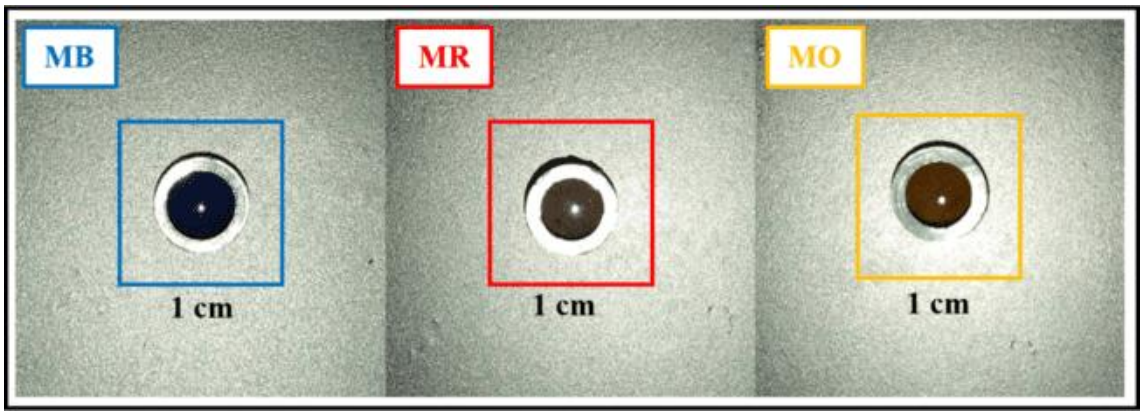

Figure 13. Cross-sectional photographic images of the phantom imaging area for methylene blue (left), methyl red (middle) and methyl orange (right).

The first analysis was conducted to apprehend the photoacoustic emission distribution characteristic from each dye solution-based phantom. The mentioned feature above can be displayed through a one-dimensional cross-sectional PA amplitude profile of the objects. The cross-sectional photoacoustic amplitude profile of each phantom with four (4) different concentration levels (10 ppm, 25 ppm, 50 ppm, and 100 ppm) is presented in Figure 14 to Figure 17, respectively. Overall, it can be stated that methyl orange solutions have the highest photoacoustic emission amplitude profile compared to the other two because of the much greater absorption on the 450 nm laser wavelength. The condition appears to be the same for every concentration level starting from 10 ppm to 100 ppm. Based on the findings above, the absorbance characteristics and concentration level of contrast agents play a significant role in generating photoacoustic emissions.[12,13]. The above statement is the main reason why methyl orange had the highest measured PA signal.

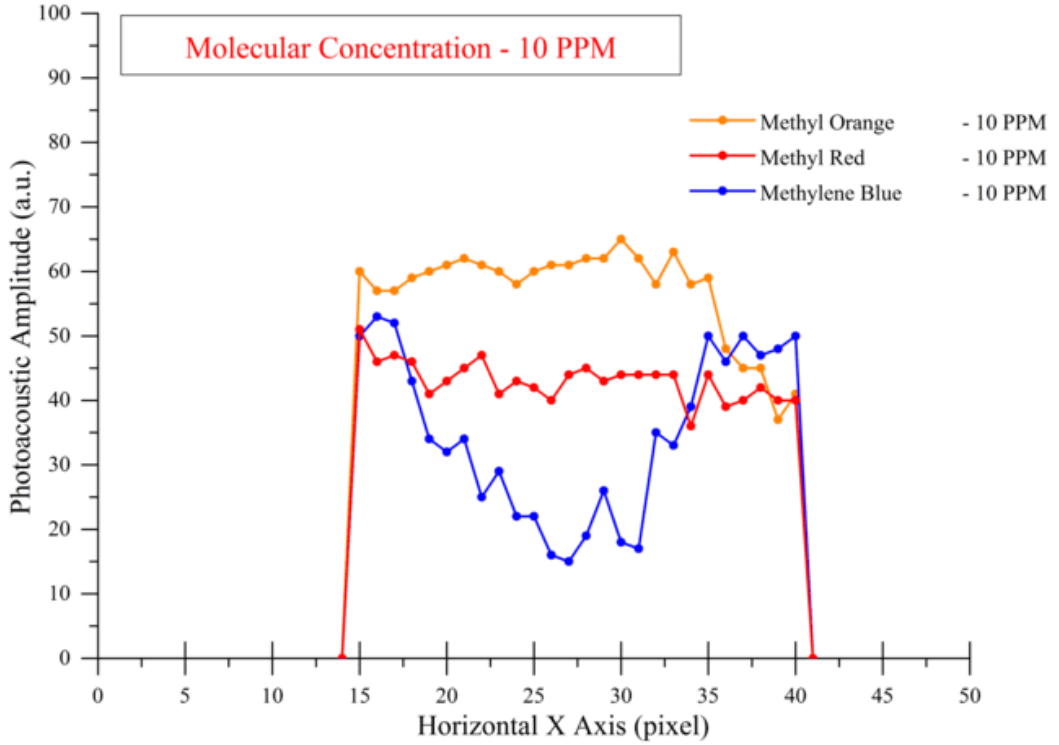

Figure 14. One-dimensional (ID) cross-sectional photoacoustic amplitude profile of the three phantom images with a molecular concentration level of 10 ppm.

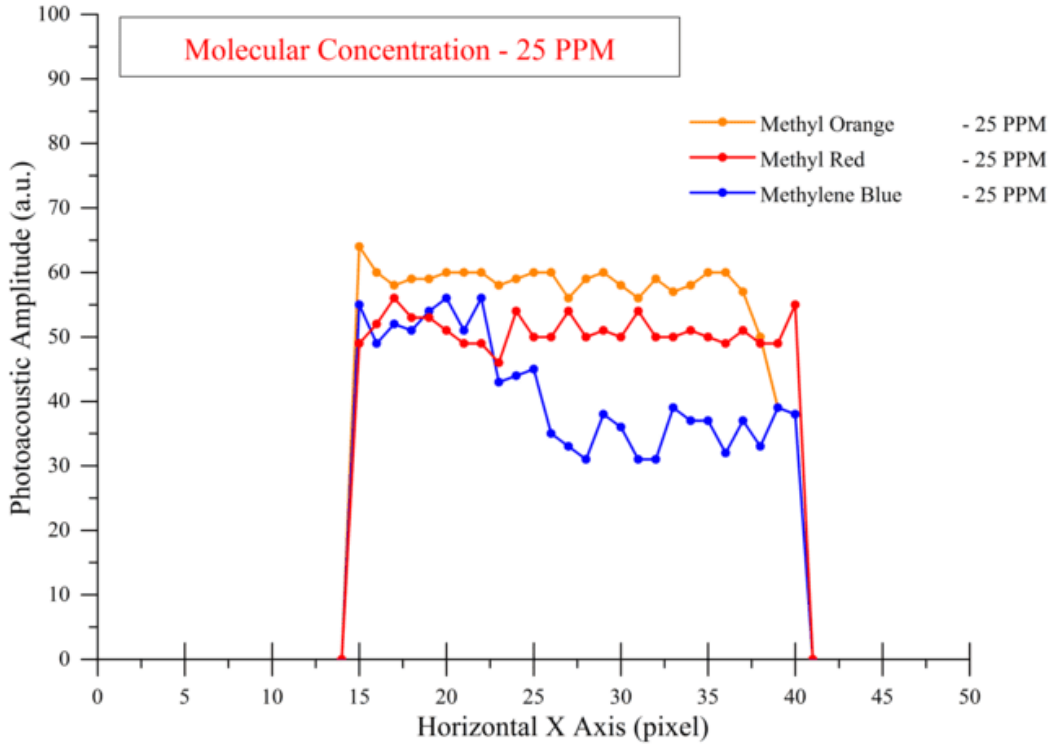

Figure 15. One-dimensional (1D) cross-sectional photoacoustic amplitude profile of the three phantom images with a molecular concentration level of 25 ppm.

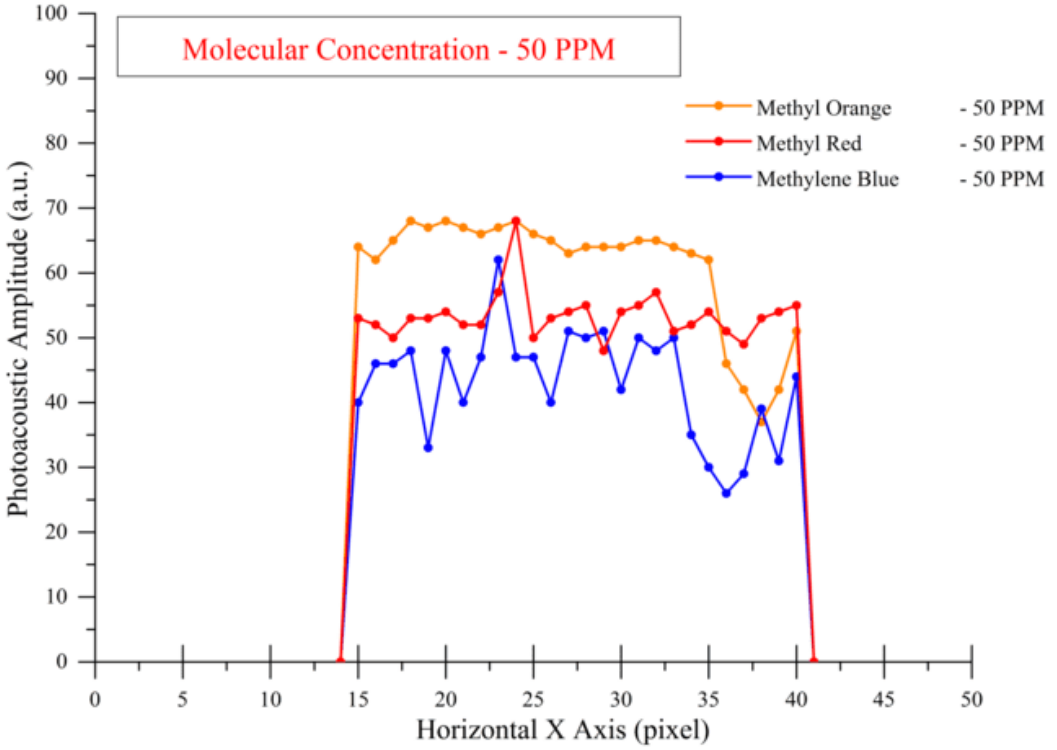

Figure 16. One-dimensional (1D) cross-sectional photoacoustic amplitude profile of the three phantom images with a molecular concentration level of 50 ppm.

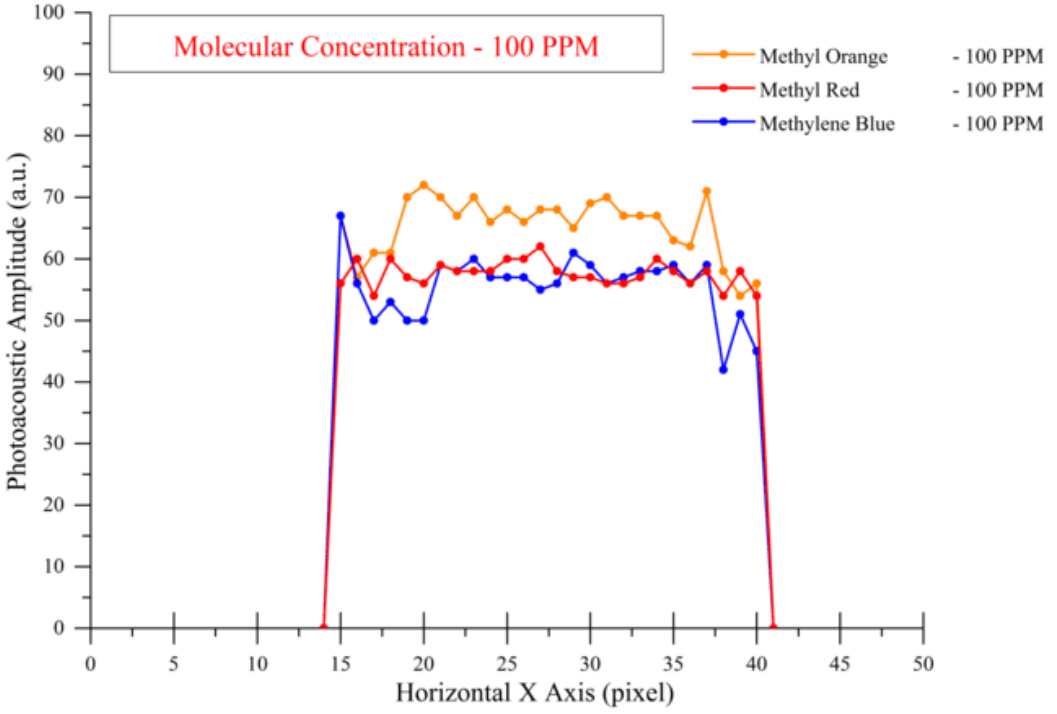

Figure 17. One-dimensional (1D) cross-sectional photoacoustic amplitude profile of the three phantom images with a molecular concentration level 100 ppm.

Figure 13 show the obtained 100 ppm methylene blue phantom image can be stated to have a pretty decent resolution. The boundary between the dye solution and the tube wall

can also be seen clearly with good contrast. Likewise, the 100 ppm methyl orange photoacoustic image also shows similar characteristics. However, the noise and distortion level is higher than the previous image.

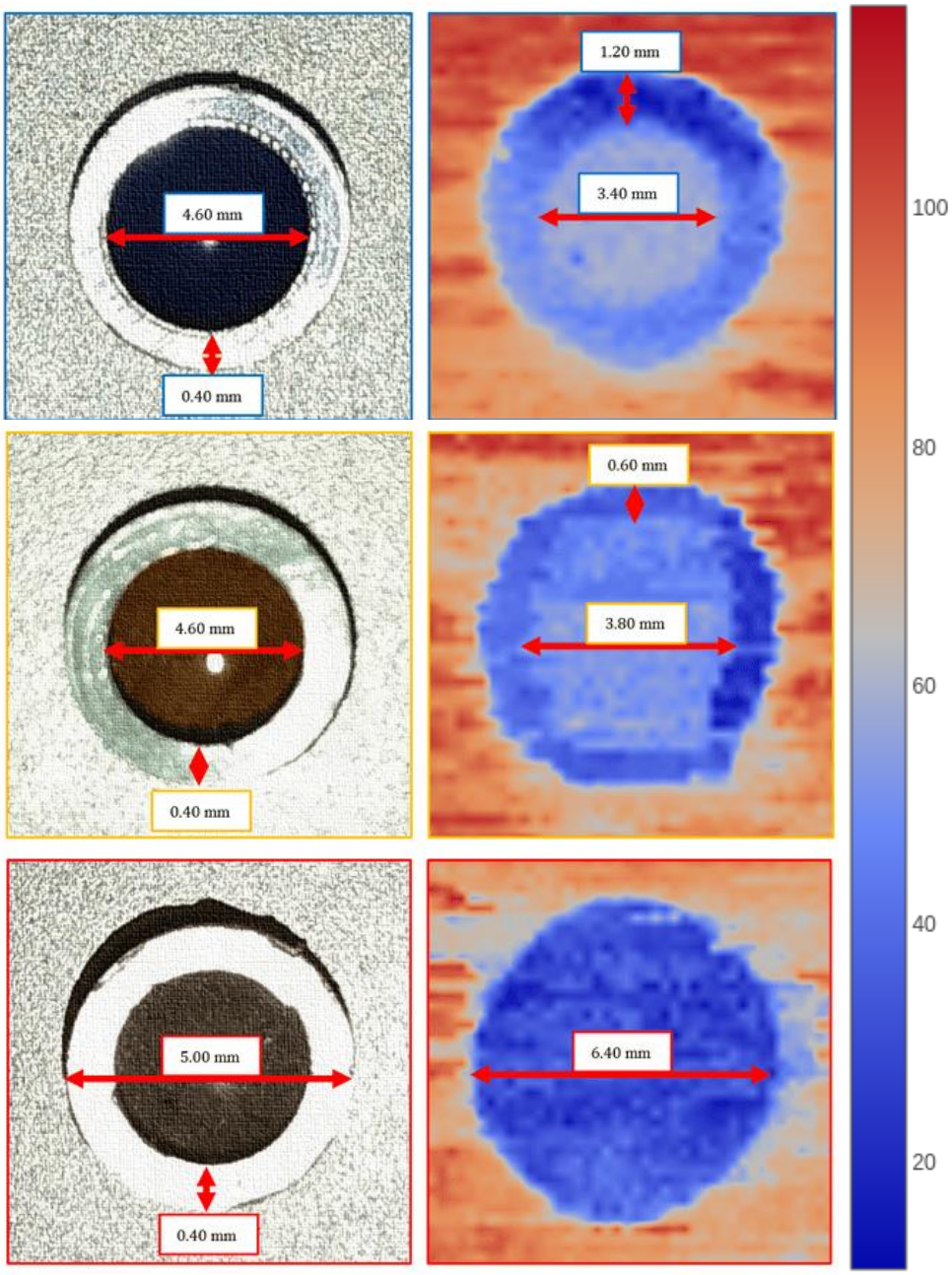

Figure 18. Phantom photographic image (left side) and PA image (right side) of 100 ppm methylene blue, methyl orange and methyl red solution along with its geometric information.

On the other hand, the PA image of 100 ppm methyl red solution shows different characteristics from the two previous images. As in Figure 13, it can be seen that the boundaries separating the two objects — the dye solution and the tube wall — cannot be directly validated by naked eyes at all due to the indistinguishable contrast of the two objects. This condition occurs because of the high PA emission uniformity between the

solution and the surrounding tube wall. The mentioned uniformity means that both the MR solution and the nylon emit PA signals with similar amplitude resulting in homogenous contrast in the obtained PA image. Hence, it can be stated that MR solutions with a particular concentration level (100 ppm) and nylon are believed to have identical photoacoustic emission characteristics at 450 nm.

Based on determining calculations, the ratio of inner tube diameter (ID) and tube wall thickness (WT) between the methylene blue and methyl orange phantom images to the original object were around 1:0.83 and 1:0.74 (ID) and 1:3 and 1:1.5 (WT), respectively. On the other hand, the only available geometric information in methyl red phantom images was only the ratio of the outer tube diameter (OD), which is around 1: 1.28. It should be noted that the data used in those calculations comes from a certain point on the coordinate axis $\vec{X}$ (ID and OD) and $\vec{Y}$ (WT) as shown in Figure 13.

From the resulting PA images shown above, it can be concluded that the difference in contrast directly represents the difference in the amplitude/strength of the photoacoustic emission produced by phantoms or background media. The blue and red gradient in the images respectively shows the geometric representation of the phantom and the background medium (galvalume plate). This achieved condition allows the boundary between two objects to be differentiated clearly.

The main factor believed to affect the ID, WT, and OD ratios in PA images of each phantom was the laser beam divergence originating from the utilized semiconductor diode. When the beam hits the object (tube or dye solution), the position of the laser beam focal point is unlikely to be close enough to the laser beam waist. That condition resulted in the enlargement of the exposed surface area, reducing the acquired PA image's lateral (spatial) resolution. However, it has been suggested that visible laser diodes (PLDs), which are often used in visible PAI, have a higher focal point than LEDs. Therefore, the main option to overcome this condition is to utilize much better PLDs with high optical resolution.

CONCLUSION

The 450 nm visible light PAI system was considered able to image the dye solution-based photoacoustic phantom object with good contrast and decent resolution especially on methylene blue and methyl orange because the boundary between the dye solution and the tube wall can be differentiated clearly although there is some distortion which lowers the spatial resolution of the images. The inner diameter (ID) and wall thickness (WT) ratio between methylene blue and methyl orange phantom images to the original object are 1:0.83 and 1:0.74 (ID) and 1:3 and 1:1.5 (WT), respectively. Meanwhile, the ratio of the outer diameter (OD) of the methyl red phantom image to the original object is 1:1.28. From this experiment, it is known that the PA emission intensity will increase in proportion to the concentration of dye molecules contained in the solution. So far, methyl orange has the highest photoacoustic emission intensity compared to the other two samples.

ACKNOWLEDGEMENTS

The authors would like to thank the entire tendance staff at the Atomic and Nuclear Physics Laboratory, Physics Department, Faculty of Mathematics and Natural Sciences,

Gadjah Mada University for assisting the corresponding author throughout the whole research.

REFERENCES

1 Zhu, Y., Xu, G., Yuan, J., Jo, J., Gandikota, G., Demirci, H., Agano, T., Sato, N., Shigeta, Y., & Wang, X. 2018. Light emitting diodes based photoacoustic imaging and potential clinical applications. *Sci. Rep.*, 8 (1), 1–12.

2 Attia, A. B. E., Balasundaram, G., Moothanchery, M., Dinish, U. S., Bi, R., Ntziachristos, V., & Olivo, M. 2019. A review of clinical photoacoustic imaging: Current and future trends. *Photoacoustics*, 16, 100144.

3 Steinberg, I., Huland, D. M., Vermesh, O., Frostig, H. E., Tummers, W. S., & Gambhir, S. S. 2019. Photoacoustic clinical imaging. *Photoacoustics*, 14, 77–98.

4 Erfanzadeh, M., & Zhu, Q. 2019. Photoacoustic imaging with low-cost sources; A review. *Photoacoustics*, 14, 1–11.

5 Weber, J., Beard, P. C., & Bohndiek, S. E. 2016. Contrast agents for molecular photoacoustic imaging. *Nat. Methods.*, 13 (8), 639–650.

6 Widyaningrum, R., Agustina, D., Mudjosemedi, M., & Mitrayana. 2018. Photoacoustic for oral soft tissue imaging based on intensity modulated continuous-wave diode laser. *Int. J. Adv. Sci. Eng. Inf. Technol.*, 8 (2), 622–627.

7 Bungart, B. L., Lan, L., Wang, P., Li, R., Koch, M. O., Cheng, L., Masterson, T.A., Dundar, M., & Cheng, J. X. 2018. Photoacoustic tomography of intact human prostates and vascular texture analysis identify prostate cancer biopsy targets. *Photoacoustics*, 11, 46–55.

8 Capozza, M., Blasi, F., Valbusa, G., Oliva, P., Cabella, C., Buonsanti, F., Cordaro, A., Pizzuto, L., Maiocchi, A., & Poggi, L. 2018. Photoacoustic imaging of integrin-overexpressing tumors using a novel ICG-based contrast agent in mice. *Photoacoustics*, 11, 36–45.

9 Zhong, H., Duan, T., Lan, H., Zhou, M., & Gao, F. 2018. Review of Low-Cost Photoacoustic Sensing and Imaging Based on Laser Diode and Light-Emitting Diode. *Sensors MDPI*, 18 (2264), 1–24.

10 Kalva, S. K., Upputuri, P. K., Rajendran, P., Dienzo, R. A., & Pramanik, M. 2019. Pulsed Laser Diode-Based Desktop Photoacoustic Tomography for Monitoring Wash-In and Wash-Out of Dye in Rat Cortical Vasculature. *J. Vis. Exp.*, 147, 1–6.

11 Upputuri, P. K., & Pramanik, M. 2018. Fast photoacoustic imaging systems using pulsed laser diodes: a review. *Biomed. Eng. Lett.*, 8 (2), 167–181.

12 Luke, G. P., Yeager, D., & Emelianov, S. Y. 2012. Biomedical applications of photoacoustic imaging with exogenous contrast agents. *Ann. Biomed. Eng.*, 40 (2), 422–437.

13 Wu, D., Huang, L., Jiang, M. S., & Jiang, H. 2014. Contrast Agents for Photoacoustic and Thermoacoustic Imaging: A Review. *Int. J. Mol. Sci.*, 15 (12), 23616–23639.

14 Gao, F., Kishor, R., Feng, X., Liu, S., Ding, R., Zhang, R., & Zheng, Y. 2017. An analytical study of photoacoustic and thermoacoustic generation efficiency towards

contrast agent and film design optimization. *Photoacoustics*, 7, 1–11.

15 Hariri, A., Lemaster, J., Wang, J., Jeevarathinam, A. K. S., Chao, D. L., & Jokerst, J. V. 2018. The characterization of an economic and portable LED-based photoacoustic imaging system to facilitate molecular imaging. *Photoacoustics*, 9, 10–20.

16 Arconada-Alvarez, S. J., Lemaster, J. E., Wang, J., & Jokerst, J. V. 2017. The development and characterization of a novel yet simple 3D printed tool to facilitate phantom imaging of photoacoustic contrast agents. *Photoacoustics*, 5, 17–24.

17 Falaras, P., Arabatzis, I. M., Stergiopoulos, T., & Bernard, M. C. 2003. Enhanced Activity of Silver Modified Thin-Film TiO2 Photocatalysts. *Int. J. Photoenergy*, 5 (3), 123–13.